Proceedings of Global Power and Propulsion Society
ISSN-Nr: 2504-4400
GPPS Montreal26
September 9-11, 2026
www.gpps.global

GPPS-TC-2026-0064

ADeT: a modular computer program for preliminary design and performance analysis of turbomachinery

Francesco Vaccari[1,2,*], Matteo Pini[1,2]
[1]**Propulsion & Power, Faculty of Aerospace Engineering, Delft University of Technology**
[2]**Cluster of Excellence SE²A - Sustainable and Energy Efficient Aviation**
*f.vaccari@tudelft.nl

ABSTRACT

Preliminary turbomachinery design conventionally relies on sequential procedures requiring manual reformulation of the governing equations when design variables or boundary conditions change. This limits flexibility across problem specifications and requires separate tools for design and performance analysis.

This paper presents *ADeT* (Autodiff Designer for Turbomachinery), an open-source, equation-oriented framework for preliminary design and performance analysis of turbomachinery. ADeT solves the complete set of governing equations simultaneously as a nonlinear residual system, enabling arbitrary selection of fixed parameters and free variables without manual reformulation. The framework is capable of modelling steady, adiabatic flow through rotating blade rows in axial, radial, and mixed-flow configurations, with interchangeable loss and deviation models. Spanwise flow variations can be captured by discretising the passage into multiple streamtubes coupled through radial equilibrium. Automatic differentiation via CasADi provides exact Jacobians for the nonlinear solver and gradient-based optimisation, while thermodynamic properties and their exact partial derivatives are supplied by CoolProp.

The framework is applied to two benchmark cases: performance map prediction for the NASA high-efficiency centrifugal compressor, and design map generation for a repeated-stage organic Rankine cycle axial turbine. Results agree well with experimental data and a previously validated meanline code, demonstrating the modelling capability and numerical robustness of the approach.

INTRODUCTION

Typical workflows for turbomachinery design begin with a conceptual phase, in which the meridional configuration of the machine is selected, i.e., axial, radial, or mixed-flow. This choice is generally guided by specific-speed and specific-diameter diagrams, such as those proposed by Balje and Japikse (1981), together with designer experience. The conceptual phase is followed by preliminary design, in which conservation equations are solved under the assumption of steady, adiabatic, axisymmetric flow to determine the velocity triangles and, therefore, the size and aerodynamic performance of the machine. When flow quantities are lumped at the inlet and outlet of each blade row, the approach is referred to as a *meanline method*. Three-dimensional effects can be considered by accounting for the spanwise evolution of flow quantities through multiple streamtubes along the blade span.

The selection of duty coefficients during preliminary design can be based on prior knowledge or existing guidelines, such as those proposed by Smith (1965) for axial turbines. Alternatively, stage duties can be obtained by performing a design optimisation that relies on models to estimate machine efficiency. Physics-based or empirical loss models capable of predicting the entropy generation along the process are commonly adopted.

Motivation

Although the availability of computational power has steadily increased, allowing higher-fidelity tools to be adopted earlier in the design process, the use of preliminary design methods and their accuracy remain essential. Refining a poorly chosen preliminary design with higher-fidelity tools may still lead to suboptimal final designs (Casey and Robinson, 2021), in addition to requiring expensive iterations. This is particularly relevant when dealing with novel and unconventional turbomachinery, for which scarce prior knowledge is available to the designer.

An overview of the meanline codes available in the open literature is presented in Anderson et al. (2025*a*) for axial, radial-inflow and radial-outflow turbines. The authors reported that available tools are usually developed for a specific

This work is licensed under **Attribution-NonCommercial-NoDerivatives 4.0 International (CC-BY-NC-ND)**
See: https://creativecommons.org/licenses/by-nc-nd/4.0/legalcode

turbomachine configuration and can solve either the design or the performance analysis problem. The consequence is that the choice of input duty coefficients, design variables and boundary conditions is rigidly determined, making such tools impractical to extend for novel applications and system layouts. Examples include turbomachinery design for fuel cell propulsion or organic Rankine cycles (ORC) for waste heat recovery (WHR) applications.

Notable examples of modern meanline tools that overcome such limitations are those documented in Jones (2015) and Anderson et al. (2024). The closed-source *Object-oriented Turbomachinery Analysis Code* (OTAC) by NASA (Jones, 2015) is only available as part of the NPSS framework (Lytle, 2000) and is capable of addressing axial, radial and mixed-flow machine configurations. The underlying system of nonlinear equations is solved by a general-purpose Newton-Raphson-based solver.

An open-source academic alternative to OTAC is *TurboFlow* (Anderson et al., 2025*b*), which can be used for both design and analysis of axial turbines, and includes performance analysis of centrifugal compressors. Although the system of governing equations is solved using a residual formulation, different machine configurations are treated separately.

The current paper presents *ADeT* (Autodiff Designer for Turbomachinery), an open-source, fully equation-oriented computer program to design and analyse the performance of arbitrary turbomachinery configurations. Unlike classical meanline models, ADeT can account for three-dimensional effects by modelling multiple non-interacting streamtubes along the blade span. The tool is developed in *Python* in order to be cross-platform and easily extensible by the community.

METHODOLOGY

The set of meanline equations describing the thermodynamic and kinematic state of a steady, adiabatic, axisymmetric flow across a blade row can be written synthetically as:

$$\dot{m}_1 = \dot{m}_2 \tag{1}$$

$$\Delta h_t = U_1 V_{\theta,1} - U_2 V_{\theta,2} \tag{2}$$

$$s_2 = s_1 + \Delta s \qquad \Delta s = f_s(\xi_1, \xi_2) \tag{3}$$

$$\beta_2 = \beta_{g,2} + \delta \qquad \delta = f_\delta(\xi_1, \xi_2) \tag{4}$$

$$f_V(\mathbf{U}_i, \mathbf{V}_i, \mathbf{W}_i) = \underline{0} \tag{5}$$

$$f_{\text{geo}}(H_1, H_2, r_1, r_2, \beta_{g,1}, \beta_{g,2}, \Gamma, \varphi_1, \varphi_2, c, c_{ax}) = \underline{0} \tag{6}$$

where ξ are vectors containing the full set of thermodynamic, kinematic and geometric quantities.

- Equation 1 imposes mass conservation across the control volume.
- Equation 2 is the Euler work equation, which represents the conservation of angular momentum across a control volume enclosing a rotating duct in steady-state and adiabatic conditions (Dixon et al., 2025).
- Equation 3 represents all the terms that generate irreversibilities within the rotating passage.
- Equation 4 accounts for the deviation of the relative flow downstream of the blade compared to the metal angle.
- Equation 5 imposes velocity triangle relationships between the the relative and absolute frames of reference, as shown in Fig. 1a
- Equation 6 represents a simplified description of the camberline and meridional geometry, linking lumped quantities to a simplified geometrical description of the blade. The geometry model used in this work consisted of parabolic camberlines, defined in the blade-to-blade plane, coupled with a meridional geometry made up of bezier curves linking straight leading and trailing edges.

By applying Eqs. 2–6 to N axisymmetric control volumes stacked in the spanwise direction, each representing a streamtube, the method can be extended to account for the spanwise evolution of the flow. Each streamtube is approximated by a mean stream surface placed at its midpoint, assuming no exchange of mass, momentum, or energy across streamtubes. Interactions between adjacent streamtubes are computed only through the geometric constraints of Eqs. 7–9 and radial equilibrium. Streamlines are assumed to be parallel to each other and perpendicular to the reference surface at the points of computation, meaning that streamline curvature effects are neglected. A schematic representation of the geometrical model is shown in Figs. 1b–1c.

$$r_i + \frac{b_i + b_{i+1}}{2} \cos\varphi = r_{i+1} \qquad i = 1, ..., (N-1) \tag{7}$$

$$r_1 = r_{\text{hub}} + b_1/2 \tag{8}$$

$$\sum_{i=1}^{N} b_i = H \tag{9}$$

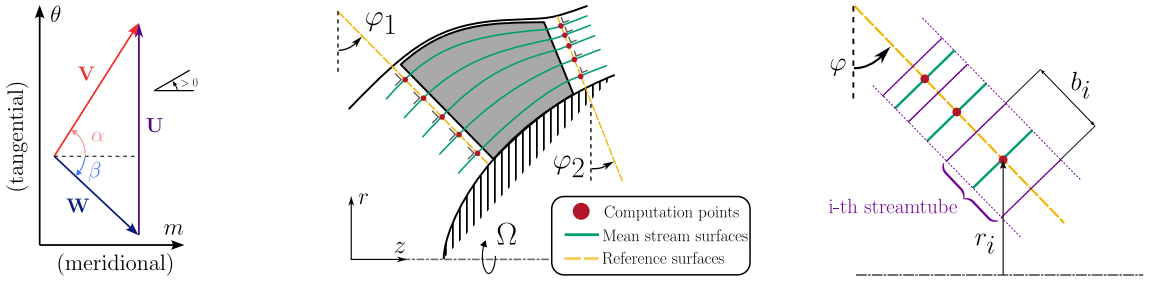

(a) Angle definitions and relationship between absolute and relative velocities.

(b) Stream surface topology in the meridional channel

(c) Reference surface placement and streamtube stacking

Figure 1 Schematic illustration of the geometric and kinematic modelling assumptions.

This geometric formulation allows modelling of turbomachinery configurations with meridional channels of arbitrary shape. However, the accuracy of the results is dictated by the availability of entropy generation models that are not machine-specific, such as those in Wallace et al. (1976).

Numerical formulation and fluid model

To achieve flexibility and modularity, a so-called *equation-oriented* (EO) modelling paradigm was adopted. This approach consists of formulating the full set of equations, as described above, as n residual equations in the form of Eq. 10. The system can be expressed as a vector function $\mathbf{F}$ of the vectors of unknowns ($\mathbf{x}$) and fixed quantities ($\mathbf{q}$). All quantities and equations are scaled by a factor based on their physical units. Depending on the choice of input parameters, the root of Eq. 11 provides either the design of the machine or its off-design performance. Within this formulation, all quantities can be treated interchangeably as either fixed parameters or free unknowns. Every relationship, entropy generation model, or definition is expressed as a residual equation, enabling high flexibility in problem definition.

$$f_k(x_1,...,x_n,q_1,...,q_m) = 0 \quad k = 1,...,n \tag{10}$$

$$\mathbf{F}(\mathbf{x},\mathbf{q}) = 0 \tag{11}$$

As a concrete example, consider specifying the specific work Δh_t directly, together with an appropriate set of dimensional boundary conditions that close the system. The dimensional residuals of Eqs. 2–5 are square (number of equations is equal to number of unknowns) and well-posed, and their root yields a dimensional design or operating point. If, instead, one wants to prescribe the loading coefficient $\psi = \Delta h_t / U_2^2$, the additional residual equation

$$\psi U_2^2 - \Delta h_t = 0 \tag{12}$$

is appended to the system, introducing ψ as a new unknown so that the system remains square. It is then possible to release the fixed condition on Δh_t and instead impose a fixed value of ψ. The nonlinear solver satisfies Eq. 12 simultaneously with all other residuals, yielding the same solution as if Δh_t had been specified directly. The same principle applies to any algebraic constraint without requiring manual reformulation of the governing equations. This leads to a modular definition of duty coefficients and entropy generation models, and allows arbitrary boundary conditions to be imposed. It also naturally handles both design and performance analysis problems through a simple selection of different sets of fixed and free variables, starting from a single declarative formulation of the problem.

A further advantage of the residual formulation is that $\mathbf{F}$ is a pure function of its inputs, enabling the application of automatic differentiation (AD) to the system. The open-source tool CasADi Andersson et al. (2018) was used for symbolic representation of the system and AD, as well as an interface to the nonlinear solver KINSOL (Lab., 1998) and the optimiser IPOPT (Wächter and Biegler, 2005). CasADi also tracks the sparsity structure of the system, including that of external function calls (i.e. equation of state computations), which can be significant as the size of the problem increases for fast evaluations of the residual function and its Jacobian.

ADeT supports arbitrary equations of state through the CoolProp thermodynamic library (Bell et al., 2014). Variables used for thermodynamic calculations during the solution process of the nonlinear system can be chosen from any of the supported input pairs. Considering, for example, pressure and temperature as independent variables, the value of any remaining fluid property y_i and its derivatives at the i-th reference surface can be computed as:

$$y_i = \mathrm{EoS}(p_i, T_i) \tag{13}$$

$$\left.\frac{\partial y_i}{\partial p}\right|_T = \mathrm{EoS}_I(p_i,T_i) \quad \left.\frac{\partial y_i}{\partial T}\right|_p = \mathrm{EoS}_{II}(p_i,T_i) \tag{14}$$

where EoS, EoS_I and EoS_{II} denote CoolProp native functions for computing property y and its partial derivatives. Second-derivative support is also implemented for the relevant thermodynamic quantities. Each time an expression containing y is differentiated, the derivative value is retrieved from the external library and embedded within the exact Jacobian computed by AD. This eliminates the overhead and inaccuracies associated with finite-difference evaluations, both for gradient-based optimisation and Jacobian computation during nonlinear solution steps. Alternatively, an ideal gas formulation is also implemented, for which the residual equations become fully algebraic.

Initial guess strategy

The goals of this work were to verify the equivalence between sequential and current equation-oriented formulations and to investigate the numerical stability of the latter when applied to canonical turbomachinery problems. Since all equations are solved simultaneously, the choice of the initial guess $\mathbf{x}_0$ is critical and can heavily influence the outcome of the nonlinear solver (Casella and Bachmann, 2021).

In order to improve the quality of the guess provided to the linear solver for all $x_k \in \mathbf{x}$, each variable that is declared within the equations is accompanied with a guess value. This procedure is partially automated and bases the guess values on the physical type of the variable. For example, if two different free variables x_i, x_j both represent a tangential velocity at different flow stations, their guess value will be the same, and this value needs to be declared only once. Guess values for the most common variables in typical turbomachinery problems are already built-in with plausible orders of magnitude. Default values can be manually overridden, either globally (for all variables of a certain type) or only targeting specific variables at a certain flow station.

For improving convergence success rates for problems for which no prior solution is available, the computation can first be run in isentropic single-span mode. This simplified solution can thus be fed to the multi-span system with loss and deviation models enabled. These models can cause convergence issues due to their high nonlinearity and/or discontinuous nature. Once a converged solution is obtained, to generate either performance or design maps, the strategy is to initiate the solver from the closest converged solution, progressively building out the map.

Problem scaling and bounding

Each variable declares its own unit, allowing to verify the unit compatibility of the sequence of operations between quantities within the equations. The unit check acts not only as a safeguard when implementing new equations, but also allows to compute the unit of each residual equation f_k. Once the units of residuals and free variables are known, it is possible to choose their scaling factors, P_k and ν_k respectively, and to rescale the problem as shown in Eq. 15.

$$x_k = \tilde{x}_k \nu_k \;\Rightarrow\; \frac{1}{P_k} f_k(\tilde{x}_1 \nu_k, ..., \tilde{x}_n \nu_n, q_1, ..., q_m) = 0 \qquad k = 1, ..., n \tag{15}$$

$$\tilde{\mathbf{F}}(\tilde{\mathbf{x}}, \mathbf{q}) = 0 \tag{16}$$

An adequate scaling of the problem is particularly important when dealing with equation-oriented formulations and can have a significant impact on the convergence of nonlinear solvers (Casella and Braun, 2017). For particularly bad initial guesses and difficulty in obtaining converged solutions, IPOPT (Wächter and Biegler, 2005), which is an optimiser by design, was used as a root-finder. This was done by setting the objective function to 0 and the residual equations as equality constraints. The advantage of IPOPT is the possibility of imposing lower and upper bounds on the iteration variables (Eq. 17), with barrier terms added to the objective preventing the variables from violating these bounds.

$$\tilde{\mathbf{x}}_{\text{lb}} \leq \tilde{\mathbf{x}} \leq \tilde{\mathbf{x}}_{\text{ub}} \tag{17}$$

Based on empirical observations, bounding strongly improved successful convergence, especially when providing lower bounds to thermodynamic update properties and a minimum meridional velocity magnitude to avoid converging to trivial solutions with null mass flow. Numerical values for guesses and bounds for several variable types can be found in the appendix.

RESULTS

The tool was tested for two typical turbomachinery applications. First, a performance analysis of a centrifugal compressor was carried out and compared to experimental data. Then, a design map was generated for a repeated stage of an organic Rankine cycle (ORC) multi-stage axial turbine, reproducing an existing design methodology for which a URANS validated point is available. The main goal of the work is to demonstrate correct model implementation and robustness of the methodology, therefore absolute accuracy was not strictly the end goal. Comparing the resulting trends and successful convergence of the problem across realistic cases had the aim of demonstrating the flexibility of the tool and its viability for potential applications of interest.

Performance map prediction for centrifugal compressors

The tool was first validated against the NASA high-efficiency centrifugal compressor (HECC) in its vaneless diffuser configuration, using experimental data from its public archive, as described, for example, by Harrison et al. (2023). In particular, the impeller data was used for comparison. The station numbering follows the convention where subscript 1 denotes the impeller inlet and 2 the impeller outlet. Uniform velocity with no inlet swirl was imposed at station 1, while the static pressure at the impeller outlet was assumed spanwise-uniform at station 2 to satisfy radial equilibrium. The effects of radial equilibrium are shown in Fig. 2a. A summary of the input parameters used for the problem setup is shown in Tab. 1. For a single spanwise station, the problem size is square (number of equations equals the number of free variables) with $|\mathbf{x}| = 118$. For 5 spanwise stations, $|\mathbf{x}| = 462$.

$T_{t,1}$	$p_{t,1}$	α_1	$r_{1,\text{hub}}$	$r_{1,\text{tip}}$	r_2	$\beta_{g,1\text{hub}}$	$\beta_{g,1\text{mid}}$	$\beta_{g,1\text{tip}}$	$\beta_{g,2}$	Z_{bl}	Z_{spl}	c_{ax}
288.16 K	101353 Pa	0°	40.64 mm	107.68 mm	215.9 mm	33 °	44 °	56 °	30 °	15	15	133.88 mm

Table 1: ***Summary of the parameters fixed for the setup of HECC performance prediction case.***

The choking point was predicted by considering an isentropic and constant-radius expansion between the inlet and the section just downstream of the impeller's leading edge, which is assumed to act as the throat of the passage. The throat area needed to account for the thickness and blade angle variation along the span. The HECC dataset provides the hub and tip thicknesses, as well as the blade angle at the hub, midspan and tip sections. These quantities were interpolated linearly, and the throat area was approximated by the average suggested by Casey and Robinson (2021), obtained by dividing the span into $N_{\text{th}} = 20$ sections and using Eq. 18. This formulation implies that choking always occurs at the inlet throat section, which is reasonable for a centrifugal compressor followed by a vaneless diffuser, although potential vaned diffuser choking would otherwise also need to be accounted for.

$$A_{\text{th}} = \frac{H_1 Z_{\text{bl}}}{N_{\text{th}}} \sum_{i=1}^{N_{\text{th}}} \left(\frac{\pi r_i}{Z_{\text{bl}}} \cos \beta_{g,1} - t_{\text{LE},i} \right) \tag{18}$$

The entropy generation models used to estimate losses across the impeller are reported in Tab. 2. All of the listed models were developed for a meanline approach; therefore, their contributions were computed using average values of thermodynamic and kinematic quantities along the span, with the exception of incidence losses, for which the model appropriately accounts for the local flow angle at each streamtube.

Mechanism	**Model**	**Coefficients**
Slip	von Backström (2005)	$F = 5$
Mixing	Johnston and Dean (1966)	$\varepsilon_w = 0.4$
Incidence	Galvas (1973)	$C_{\text{inc}} = 1.0$
Tip clearance	Jansen (1970)	$\tau = 0.2694$ mm
Skin friction	Jansen (1970)	c_f from Aungier (2000)
Disk friction	Daily and Nece (1960)	$\tau_d = 1$ mm
Blade loading	Coppage and Dallenbach (1956)	$C_{\text{load}} = 0.75$
Recirculation	Coppage and Dallenbach (1956)	-
Choking	Aungier (2000)	C_r=1

Table 2: ***Slip and entropy generation models used for loss accounting in the centrifugal compressor model.***

Each loss contribution was computed in terms of a total enthalpy loss, which was then converted to entropy generation using the isentropic outlet temperature as reference, as shown in Eq.19.

$$\Delta s_{\text{losses}} = \frac{\Delta h_{t,\text{losses}}}{T_{2,s}} \qquad T_{2,s} = \text{EoS}(p_2, s_1) \tag{19}$$

The empirical coefficients used for tuning the loss models are also reported in Tab. 2 and their chosen values align with suggested values in the original works. The predicted performance maps were compared for total-to-total pressure ratio and isentropic efficiency in Fig. 3, against experimental data; the coloured bands representing a $\pm 2\%$ error band with respect to the computed values.

The agreement with the experimental data is satisfactory across the operating range, although the accuracy of these legacy loss models is expected to falter when applied to modern compressors. The orders of magnitude of the total-to-total

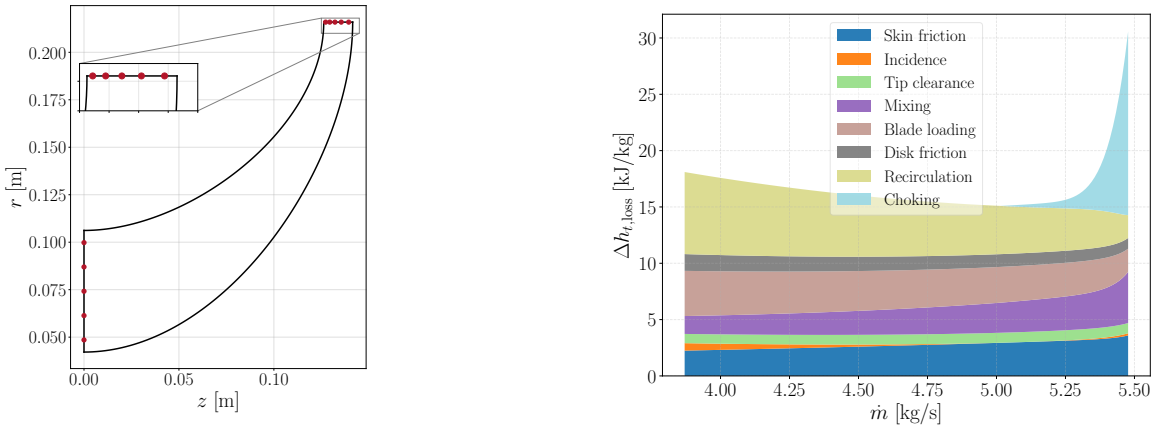

(a) Meridional view of the impeller showing the effects of radial equilibrium on the spanwise distribution of the mean stream-tubes.

(b) Spanwise-averaged loss breakdown for the 20,000 rpm speedline.

Figure 2 Radial equilibrium effects and loss breakdown for the NASA HECC case.

pressure ratio are correct, but the slope variation across different speedlines is not captured. The efficiency trends show very good agreement, although it must be recognised that the experimental measurements seem to stop far away from the actual choking point; therefore, it remains difficult to judge the validity of the choking prediction and the extent of the operating range.

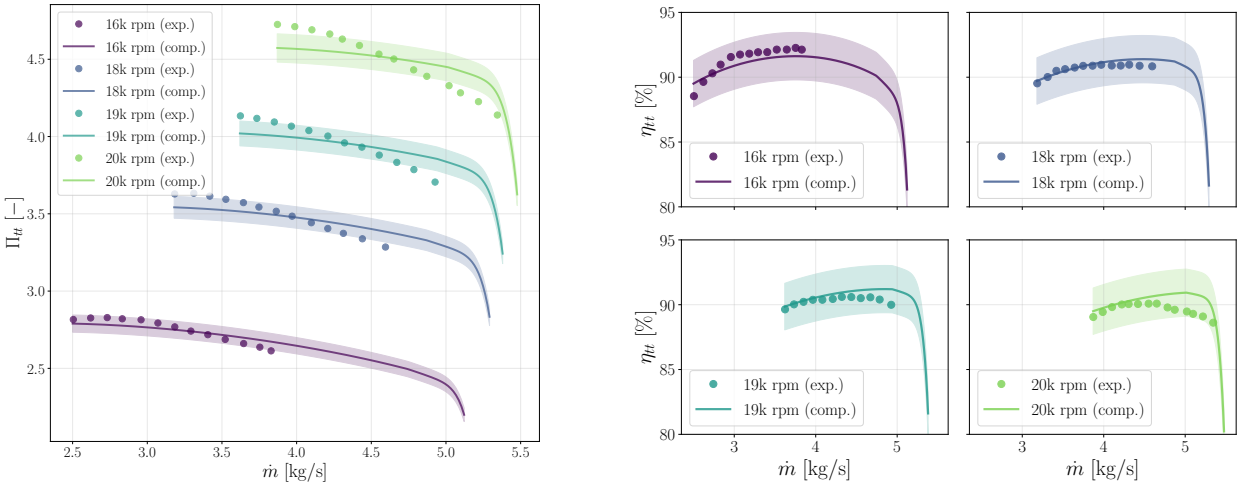

(a) Total-to-total impeller pressure ratio

(b) Total-to-total impeller efficiency

Figure 3 NASA HECC impeller predicted performance maps compared to experimental data (Harrison et al., 2023) in its vaneless configuration. Coloured bands represent a $\pm 2\%$ error band with respect to the computed values.

Design map for axial turbine operating with non-ideal compressible flows

The axial turbine design capability of the tool was verified by reproducing one of the design maps reported in Giuffre' and Pini (2021), which were generated using *TurboSim*, a meanline code previously developed within the research group. The working fluid was siloxane MM, with total reduced inlet conditions representative of turbines for high-temperature organic Rankine cycle (ORC) power systems, summarised in Tab. 3. A repeated-stage configuration was assumed, with the following conditions enforced:

$T_{t,1\ \mathrm{red}}$	$p_{t,1\ \mathrm{red}}$	χ	ϕ	K_{is}	$\mathrm{Zw}_{\mathrm{rot}}$	$\mathrm{Zw}_{\mathrm{stat}}$	$r_{\mathrm{hub}}/r_{\mathrm{tip}}$	$\rho_{t,1}/\rho_3$	t_{TE}/l	δ^*/θ	θ/t_{TE}	δ^*_{EW}/H	τ/H	c_{ax}
1.045	1.3	0.3	0.55	3.0	0.85	0.85	0.818	4	0.02	2	0.075	0.05	0.01	3.0

Table 3: ***Summary of the parameters fixed for generating the design map in the ORC turbine case.***

$$\alpha_1 = \alpha_3 \qquad V_m = \text{const} \qquad \bar{r} = \text{const} \tag{20}$$

where subscript 1 denotes the stator inlet, 2 the stator outlet and rotor inlet, and 3 the rotor outlet.

A simple parabolic camberline was used to provide a first estimate of the arc length, required for the surface integrals in the profile loss and tip clearance models. The axial chord of the blade was set by imposing an aspect ratio of AR = 3.0, subject to the constraint that the flare angle did not exceed 30°:

$$c_{ax} = \min\left(\frac{H_{\text{in}} + H_{\text{out}}}{2\text{AR}}, \frac{\Delta H}{\tan 30^\circ}\right) \tag{21}$$

The stage volumetric flow ratio, the hub-to-tip radius ratio at the stator outlet, and the degree of reaction were fixed as per the original work, with values reported in Tab. 3. The number of blades was determined from the Zweifel criterion, as defined by Coull and Hodson (2011), for both the stator and the rotor.

Given the high hub-to-tip ratios of such a machine, only a meanline design was carried out, namely the calculation was performed assuming a single streamtube. Applying the design routine directly to a multi-streamtube formulation was found to cause frequent convergence failures across the design map. Instead, the design and efficiency evaluation were carried out at midspan, with a free-vortex blade design then applied along the blade span. A summary of the parameters is given in Tab. 3; the resulting system from this setup leads to a size of $|\mathbf{x}| = 230$.

Physics-based loss models were used throughout, with the exception of secondary flow losses, which were estimated based on a semi-empirical correlation. The models are summarised in Tab. 4. Shock losses were incorporated within the mixing loss model, which was derived from a control-volume approach and the semi-empirical base pressure correlation by Sieverding et al. (1979). Incidence and deviation effects were assumed to be negligible, since the maps were computed only at the design point.

Mechanism	Model	Coefficients
Mixing	Denton and Xu (1989)	C_{pb} from Sieverding et al. (1979)
Profile	Denton (1990)	$C_d = 0.002$
Tip clearance	Denton (1993)	$C_{\text{disch}} = 0.35$
Secondary flow	Benner et al. (2005)	–

Table 4: ***Loss models used to generate the axial turbine design maps.***

The design space was parameterised using the total-to-static isentropic loading coefficient K_{is} and the flow coefficient ϕ, defined in Eq. 22. The flow coefficient was varied between 0.4 and 1.4, while the loading coefficient was varied between 3 and 10.

$$K_{is} = \frac{2\,(h_{t,1} - h_{t,3s})}{U^2} \qquad \phi = \frac{V_m}{U} \tag{22}$$

The geometrical scaling followed Giuffre' and Pini (2021); the physical problem was solved using dimensional equations, and the result was a machine geometry scaled by an arbitrary mean radius. Scaling effects were not considered; therefore, the absolute value of the mean radius had no effect on performance predictions. The resulting design map is shown in Fig. 4.

For this combination of fluid and inlet conditions Giuffre' and Pini (2021) reported a URANS-validated efficiency of 93.75% for the stage design characterised by $\phi = 0.55$, $K_{is} = 3.0$, while *ADeT* predicted 93.66%. A systematic CFD validation across the full design map was not carried out and remains an avenue for future work.

The calculation of the map was carried out according to the following numerical strategy: once a solution for a single design point was obtained, the solution of the non-linear problem of the other design points on the map converged satisfactorily, with each new design problem initialised from the nearest converged solution. It should be noted, however, that the convergence of the first design point could be particularly challenging, especially near the bounds of the design space. In order to improve the convergence of the root-finding algorithm, the thermodynamic variables were bounded within a reasonable interval based on the inlet flow conditions.

CONCLUSIONS AND OUTLOOK

This paper presents *ADeT*, an open-source Python tool for meanline design and performance analysis of turbomachinery. It is shown that the canonical turbomachinery meanline problem can be reformulated as a residual-based system. This offers the advantage of defining the boundary conditions, duty coefficients, and loss models in a flexible manner without the need to change the solution procedure of the governing equations, and provides a single unified model for both design and

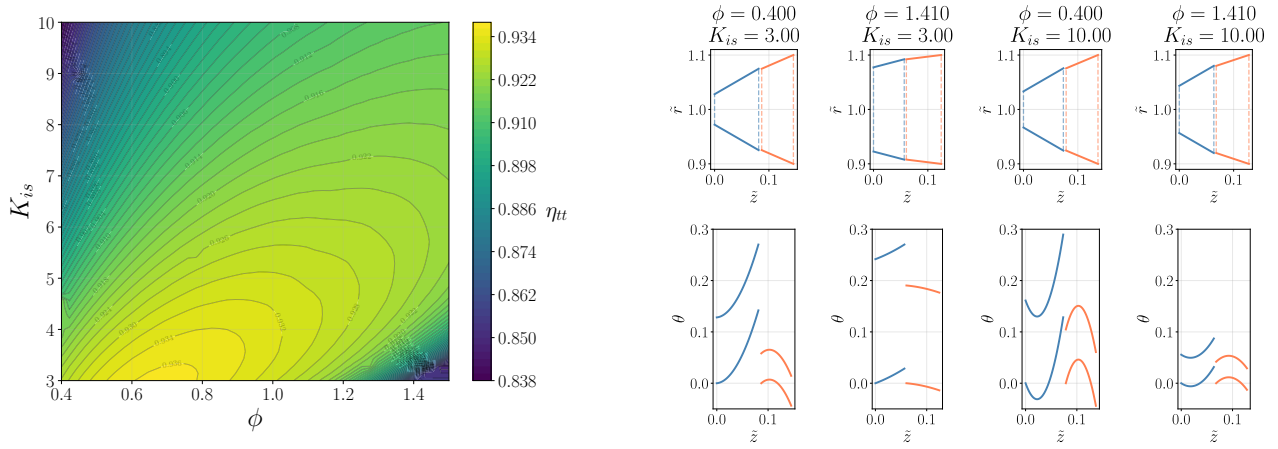

(a) Total-to-total isentropic efficiency as a function of flow coefficient and isentropic loading coefficient

(b) Representative meridional channel and camberline geometries across the design map

Figure 4 Design maps for a repeated-stage axial turbine operating with siloxane MM

performance analysis problems. Turbines and compressors of different types (axial, radial or mixed-flow) can be treated by swapping the set of equations describing the entropy generation and flow deviation models, although the current model library still remains limited in that regard. Automatic differentiation, implemented via CasADi, yields exact Jacobian matrices at negligible computational cost relative to finite-difference approximations. This eliminates numerical differentiation errors during nonlinear solution steps and makes *ADeT* directly applicable to gradient-based optimisation without code modification.

The tool was assessed against two case studies: a performance map of a centrifugal compressor and the generation of a design map of a repeated stage axial turbine for ORC applications. The benchmarks qualitatively demonstrate the flexibility of the formulation in terms of handling different machine types for analysis and design problems. For the NASA high-efficiency centrifugal compressor (HECC), the predicted total-to-total pressure ratio and efficiency maps match the experimental data (Harrison et al., 2024) satisfactorily across multiple speedlines. For a repeated-stage ORC axial turbine, *ADeT* predicts a design-point total-to-total efficiency of 93.66% for a stage characterised by $\phi = 0.55$, $K_{is} = 3.0$, compared to the reference value computed by URANS of 93.75% reported by Giuffre' and Pini (2021). This comparison is limited to a single point; a systematic CFD validation across the full design map was not carried out and remains an open point. While quantitative comparisons against experimental and high-fidelity data are satisfactory for the chosen benchmarks, more methodical investigations against established tools remain an open question. The accuracy and validity of the loss models is specific to the set of applications that were analysed, therefore the applicability of the tool to a wider range of problems is not yet demonstrated, e.g.: axial turbine off-design performance prediction, design and analysis of mixed-flow machines, radial-inflow turbines.

The current implementation does not yet support the modelling of components in which the flow is described by ordinary differential equations, such as in detailed vaneless diffuser models or inter-row mixing models; their addition requires the treatment of differential-algebraic equations (DAE) in the solution procedure, and is the subject of ongoing development. Gradient-based design optimisation, enabled by the exact sensitivities provided by automatic differentiation, is already implemented but has not yet been tested systematically. *ADeT* is publicly available on GitHub.

ACKNOWLEDGMENTS

We would like to thank Prof. Francesco Casella for his help and insight into equation-oriented modelling. We also want to acknowledge C. J. Luiten and R.D. Silva Oliveira Meireles for the useful input and reference regarding centrifugal compressor models. We would like to acknowledge the funding by the Deutsche Forschungsgemeinschaft (DFG, German Research Foundation) under Germany's Excellence Strategy – EXC 2163/1 - Sustainable and Energy Efficient Aviation – Project-ID 390881007.

NOMENCLATURE

Acronyms

AD	Automatic Differentiation
AT	Axial Turbine
BC	Boundary condition
CC	Centrifugal Compressor
DAE	Differential-Algebraic Equation
EO	Equation-Oriented
HECC	High-Efficiency Centrifugal Compressor
ODE	Ordinary Differential Equation
ORC	Organic Rankine Cycle
URANS	Unsteady Reynolds-Averaged Navier-Stokes

Roman symbols

A	Area [m^2]
AR	Aspect ratio [-]
C	Coefficient [-]
F	Slip factor coefficient [-]
H	Total channel height [m]
K_{is}	Total-to-static isentropic loading coefficient [-]
M	Mach number [-]
N	Number of streamtubes [-]
P	Residual scaling factor [-]
T	Temperature [K]
U	Blade peripheral speed [m/s]
V	Absolute flow velocity magnitude [m/s]
W	Relative flow velocity magnitude [m/s]
Z_{bl}	Number of blades [-]
Z_{spl}	Number of splitters [-]
Zw	Zweifel coefficient [-]
a	Speed of sound [m/s]
b	Streamtube height [m]
c	Blade chord [m]
c_{ax}	Blade axial chord [m]
c_f	Friction coefficient [-]
h	Specific enthalpy [J/kg]
i	Incidence angle [rad]
l	Blade pitch [m]
$\dot{m}$	Mass flow rate [kg/s]
p	Pressure [Pa]
r	Radial coordinate [m]
$\bar{r}$	Mean radius [m]
s	Specific entropy [J/(kg·K)]
t	Blade thickness [m]
w	Specific work [J/kg]
z	Axial coordinate [m]

Greek symbols

Γ	Stagger Angle [-]
Ω	Rotational speed [rad/s]
Π	Pressure ratio [-]
α	Absolute flow angle [rad]
β	Relative flow angle [rad]
β_g	Blade geometrical angle [rad]
χ	Degree of reaction [-]
δ	Flow deviation angle [rad]
δ^*	Displacement thickness [m]
ε_w	Compressor wake fraction [-]
η_{tt}	Total-to-total isentropic efficiency [-]
γ	Ratio of specific heats [-]
ν	Variable scaling factor [-]
ϕ	Flow coefficient [-]
ψ	Loading coefficient [-]
ρ	Density [kg/m^3]
σ	Solidity [-]
τ	Tip clearance [m]
τ_{d}	Back face clearance [m]
θ	Momentum thickness [m]
φ	Meridional angle [rad]
ξ	State vector [-]

Subscripts

θ	Tangential component
m	Meridional component
s	Isentropic process state
t	Total (stagnation) quantity
pb	Base pressure
ax	Referred to the axial chord
1	Impeller inlet (CC); stator inlet (AT)
2	Impeller outlet (CC); stator outlet (AT)
3	Rotor outlet (AT)
in	Blade row inlet
out	Blade row outlet
rot	Rotor
stat	Stator
th	Throat section
LE	Leading edge
TE	Trailing edge
EW	Endwall

Operators

$\lvert\cdot\rvert$	Vector size
$\overline{(\cdot)}$	Mean value

References

Anderson, L. B., Agromayor, R., Haglind, F. and Nord, L. O. (2025*a*), 'Equation-oriented and black-box design optimization of axial turbines using gradient-based and gradient-free algorithms', *Journal of Turbomachinery* **148**(1). http://dx.doi.org/10.1115/1.4069468.

Anderson, L. B., Agromayor, R., Haglind, F. and Nord, L. O. (2025*b*), 'Turboflow: Meanline modelling of axial turbines', *Journal of Open Source Software* **10**(111), 7588. https://doi.org/10.21105/joss.07588.

Anderson, L. B., Agromayor, R., Parisi, S., Haglind, F. and Nord, L. O. (2024), 'Equation-oriented meanline method for axial turbine performance prediction under choking conditions', *Journal of Turbomachinery* **147**(4). http://dx.doi.org/10.1115/1.4066741.

Andersson, J. A. E., Gillis, J., Horn, G., Rawlings, J. B. and Diehl, M. (2018), 'Casadi: a software framework for nonlinear optimization and optimal control', *Mathematical Programming Computation* **11**(1), 1–36. http://dx.doi.org/10.1007/s12532-018-0139-4.

Aungier, R. H. (2000), *Centrifugal Compressors: A Strategy for Aerodynamic Design and Analysis*, ASME Press. http://dx.doi.org/10.1115/1.800938.

Balje, O. E. and Japikse, D. (1981), 'Turbomachines—a guide to design selection and theory', *Journal of Fluids Engineering* **103**(4), 644–644. http://dx.doi.org/10.1115/1.3241788.

Bell, I. H., Wronski, J., Quoilin, S. and Lemort, V. (2014), 'Pure and pseudo-pure fluid thermophysical property evaluation and the open-source thermophysical property library coolprop', *Industrial Engineering Chemistry Research* **53**(6), 2498–2508. http://dx.doi.org/10.1021/ie4033999.

Benner, M. W., Sjolander, S. A. and Moustapha, S. H. (2005), 'An empirical prediction method for secondary losses in turbines—part ii: A new secondary loss correlation', *Journal of Turbomachinery* **128**(2), 281–291. http://dx.doi.org/10.1115/1.2162594.

Casella, F. and Bachmann, B. (2021), 'On the choice of initial guesses for the newton-raphson algorithm', *Applied Mathematics and Computation* **398**, 125991. http://dx.doi.org/10.1016/j.amc.2021.125991.

Casella, F. and Braun, W. (2017), On the importance of scaling in equation-based modelling, *in* 'Proceedings of the 8th International Workshop on Equation-Based Object-Oriented Modeling Languages and Tools', EOOLT'17, ACM, p. 3–7. http://dx.doi.org/10.1145/3158191.3158192.

Casey, M. and Robinson, C. (2021), *Radial Flow Turbocompressors: Design, Analysis, and Applications*, Cambridge University Press. http://dx.doi.org/10.1017/9781108241663.

Coppage, J. and Dallenbach, F. (1956), Study of supersonic radial compressors for refrigeration and pressurization systems, Technical report, Garret Corp.

Coull, J. D. and Hodson, H. P. (2011), Blade loading and its application in the mean-line design of low pressure turbines, *in* 'Volume 7: Turbomachinery, Parts A, B, and C', GT2011, ASMEDC, p. 547–558. http://dx.doi.org/10.1115/gt2011-45238.

Daily, J. W. and Nece, R. E. (1960), 'Chamber dimension effects on induced flow and frictional resistance of enclosed rotating disks', *Journal of Basic Engineering* **82**(1), 217–230. http://dx.doi.org/10.1115/1.3662532.

Denton, J. D. (1990), Entropy generation in turbomachinery flows, *in* 'SAE Technical Paper Series', Vol. 1 of *AEROTECH*, SAE International. http://dx.doi.org/10.4271/902011.

Denton, J. D. (1993), Loss mechanisms in turbomachines, *in* 'Volume 2: Combustion and Fuels; Oil and Gas Applications; Cycle Innovations; Heat Transfer; Electric Power; Industrial and Cogeneration; Ceramics; Structures and Dynamics; Controls, Diagnostics and Instrumentation; IGTI Scholar Award', GT1993, American Society of Mechanical Engineers. http://dx.doi.org/10.1115/93-gt-435.

Denton, J. D. and Xu, L. (1989), The trailing edge loss of transonic turbine blades, *in* 'Volume 1: Turbomachinery', GT1989, American Society of Mechanical Engineers. http://dx.doi.org/10.1115/89-gt-278.

Dixon, S. L., Hall, C. and Zhao, D. (2025), *Introduction: Basic principles*, Elsevier, p. 1–46. http://dx.doi.org/10.1016/b978-0-443-29831-8.00013-9.

Galvas, M. R. (1973), Fortran program for predicting off-design performance of centrifugal compressors, Technical report, NASA.

Giuffre', A. and Pini, M. (2021), 'Design guidelines for axial turbines operating with non-ideal compressible flows', *Journal of Engineering for Gas Turbines and Power* . http://dx.doi.org/10.1115/1.0002545v.

Harrison, H. M., McNichols, E. O. and Blaha, M. R. (2023), Nasa small engine components compressor test facility: High efficiency centrifugal compressor vaneless diffuser and transition duct configurations, *in* 'ASME Turbo Expo Turbomachinery Technical Conference and Exposition', GT2023, American Society of Mechanical Engineers. http://dx.doi.org/10.1115/gt2023-103128.

Harrison, H. M., Nguyen-Huynh, T. and Mathison, R. M. (2024), Nasa hecc geometry and performance review part 3: A numerical and experimental investigation of tip clearance effects on the vaneless diffuser configuration, *in* 'Volume 12D: Turbomachinery — Multidisciplinary Design Approaches, Optimization, and Uncertainty Quantification; Radial Turbomachinery Aerodynamics; Unsteady Flows in Turbomachinery', GT2024, American Society of Mechanical Engineers. http://dx.doi.org/10.1115/gt2024-121641.

Jansen, W. (1970), 'A method for calculating the flow in a centrifugal impeller when entropy gradient are present', *Inst. Mech. Eng. Internal Aerodynamics* .

Johnston, J. P. and Dean, R. C. (1966), 'Losses in vaneless diffusers of centrifugal compressors and pumps: Analysis, experiment, and design', *Journal of Engineering for Power* **88**(1), 49–60. http://dx.doi.org/10.1115/1.3678477.

Jones, S. M. (2015), Design of an object-oriented turbomachinery analysis code: Initial results, *in* 'International Symposium on Airbreathing Engines (ISABE 2015)', number GRC-E-DAA-TN23162.

Lab., L. L. N. (1998), User documentation for kinsol, a nonlinear solver for sequential and parallel computers, Technical report, Lawrence Livermore National Lab., CA (United States). https://www.osti.gov/biblio/314885.

Lytle, J. K. (2000), 'The numerical propulsion system simulation: An overview', *Computational Aerosciences* (E-12152).

Sieverding, C. H., Stanislas, M. and Snoek, J. (1979), The base pressure problem in transonic turbine cascades, *in* 'Volume 1B: Gas Turbines', GT1979, American Society of Mechanical Engineers. http://dx.doi.org/10.1115/79-gt-120.

Smith, S. F. (1965), 'A simple correlation of turbine efficiency', *The Journal of the Royal Aeronautical Society* **69**(655), 467–470. http://dx.doi.org/10.1017/s0001924000059108.

von Backström, T. W. (2005), 'A unified correlation for slip factor in centrifugal impellers', *Journal of Turbomachinery* **128**(1), 1–10. http://dx.doi.org/10.1115/1.2101853.

Wallace, F. J., Baines, N. C. and Whitfield, A. (1976), A unified approach to the one-dimensional analysis and design of radial and mixed flow turbines, *in* 'Volume 1B: General', GT1976, American Society of Mechanical Engineers. http://dx.doi.org/10.1115/76-gt-100.

Wächter, A. and Biegler, L. T. (2005), 'On the implementation of an interior-point filter line-search algorithm for large-scale nonlinear programming', *Mathematical Programming* **106**(1), 25–57. http://dx.doi.org/10.1007/s10107-004-0559-y.

Appendix A - Numerical values for guesses and bounds by variable type

Variables without explicitly specified guesses default to a user-specified value, 0.5 was used for all cases in the present work. Variables without explicitly specified bounds default to $(-10^{20}, 10^{20})$. All values are expressed in SI units. Guess and bound values are overwritten by case-specific custom values.

Variable	Guess	L. Bound	U. Bound
M, M_{rel}	0.3		
V, W	0.5	0	$2 \cdot 10^3$
V_m, W_m	0.5	0	$2 \cdot 10^3$
U	10^{-2}		
α, β	10^{-2}	-1.5	1.5

Variable	Guess	L. Bound	U. Bound
Base pressure p_b	$3 \cdot 10^5$		
Mass flow	20.0	0	$5 \cdot 10^4$
Momentum thickness θ	10^{-5}		
Displacement thickness δ^*	$2 \cdot 10^{-5}$		
Isentropic temperature T_{is}	300		

Table 5: ***Defaults values for kinematic and miscellaneous variables***

Variable	Guess	L. Bound	U. Bound
Streamtube area	0.1		
Full annulus area	0.3		
Chords c, c_{ax}	0.1		
Blade pitch l	0.1		
Streamtube radius r_i	0.1		
Streamtube height b_i	0.1	0	10^2
Channel height H	0.3	0	10^2
Stagger Γ	0.1		
Blade thickness t	0.005		
Solidity σ	1.0		
Number of blades Z_{bl}	50.0		
Metal angle β_g	-0.3	-1.5	1.5
AR	2.0		
Tip clearance τ	0.001		
Flare angle	0.1	-1.5	1.5

Table 6: ***Default values for geometric variables***

Variable	Guess	L. Bound	U. Bound
p, p_t, $p_{t,r}$	$p_{t,1}$	100.0	10^6
T, T_t, $T_{t,r}$	$T_{t,1}$	100.0	10^6

Table 7: ***Custom guesses and bounds for the HECC performance analysis case***

Variable	Guess	L. Bound	U. Bound
p, p_t, $p_{t,r}$	$p_{t,1}$	$0.5 \cdot p_{\text{crit}}$	$1.5 \cdot p_1$
T, T_t, $T_{t,r}$	$T_{t,1}$	$0.5 \cdot T_{\text{crit}}$	$1.5 \cdot T_1$
Loss terms Δs	–	0.0	50.0
U	–	0.0	300.0
V	–	20.0	150.0

Table 8: ***Custom guesses and bounds for the ORC design map case***